Check for updates

PHYSICS

# Photonic entanglement swapping with remote quantum dots

**Mattia Beccaceci[1]†, Giuseppe Ronco[1]*†, Fabrizio Cienzo[1], Pierpaolo Bassetti[1], Alessandro Laneve[1,2,3], Francesco Basso Basset[4], Tobias M. Krieger[5], Thomas Oberleitner[5], Quirin Buchinger[6], Francesco Salusti[7], Barbara Souza Damasceno[6], Silke Kuhn[6], Saimon F. Covre da Silva[8], Sandra Stroj[9], Klaus D. Jöns[7], Sven Höfling[6], Tobias Huber-Loyola[6,10], Armando Rastelli[5], Michele B. Rota[1], Rinaldo Trotta[1]***

Copyright © 2026 The Authors, some rights reserved; exclusive licensee American Association for the Advancement of Science. No claim to original U.S. Government Works. Distributed under a Creative Commons Attribution NonCommercial License 4.0 (CC BY-NC).

**Entanglement swapping is a protocol that details how to create entanglement between previously uncorrelated particles. Its photonic version, mediated by the interference of photon pairs generated by separate quantum systems, finds disparate applications in quantum networks. So far, entanglement swapping with entangled photons from remote systems has been implemented only using probabilistic sources. However, the scaling up of quantum networks requires nonprobabilistic quantum emitters without a trade-off between the degree of entanglement and photon-pair generation rate. Here, we demonstrate photonic entanglement swapping using photon pairs generated by two separate GaAs quantum dots. The emitters are deterministically embedded in hybrid semiconductor-piezoelectric devices that make the entangled photons from two dissimilar quantum dots nearly identical. Entanglement swapping is demonstrated with a fidelity as high as 0.71(2), more than 10 SDs above the classical limit. The experimental data are quantitatively explained by a theoretical model that also suggests how to boost the protocol performance. Our work opens the path to the exploitation of quantum dot entangled-photon sources in quantum repeater networks.**

## INTRODUCTION

To develop a global quantum network (*1*), many challenges need to be addressed. One key undertaking is to efficiently generate and distribute entanglement across distant parties, bypassing the limits set by the no-cloning theorem. This task requires quantum repeaters, i.e., "devices" that mitigate the exponential loss of quantum signals over distance by teleporting entanglement between previously uncorrelated nodes. There is a plethora of approaches to quantum repeaters (*2*, *3*), ranging from those based on matter quantum memories (*4*) to those relying on multiphoton graph states (*5*). In many of them, swapping operations are used to share entanglement between remote network nodes by exploiting entanglement that is first generated locally (*6*–*8*). Over the last few decades, entanglement swapping has been implemented using different physical platforms (*9*–*15*), generating locally either atom(spin)-photon or photon-photon entanglement. The photonic version of entanglement swapping, with quantum information exclusively encoded in photons' degrees of freedom, is particularly relevant for technological applications, as communication over long distances is made efficient by directly entangling flying qubits and by the straightforward possibility of concatenating swapping operations (*3*). Moreover, efficient photon-photon entanglement swapping is also a crucial ingredient for photonic quantum computing (*16*). Following the landmark experiment of Pan *et al.* (*9*), photonic entanglement swapping has been achieved in controlled laboratory settings (*17*), on a photonic chip (*18*), in the telecom band (*19*), and in deployed field infrastructure (*20*–*22*). Yet, all these demonstrations rely on probabilistic photon sources, in which the probability of generating a single photon-pair per pulse cannot be driven over the threshold imposed by the deleterious effect of multiphoton emission on entanglement. This fundamental constraint hampers their use in information processing, as the successful generation of entanglement between separate nodes may require a very large number of attempts, even after multiplexing. For this reason, implementations based on probabilistic photon sources can hardly be scaled up to the framework of practical quantum networks.

Quantum emitters—such as atoms (*23*), quantum dots (QDs) (*24*), NV centers (*25*), and defects in two-dimensional semiconductors (*26*)—address this hurdle by delivering on-demand single and entangled photons (*27*) with negligible multiphoton emission probability (*28*). Quantum emitters can also host spin qubits, which can be entangled with the flying photons (*29*, *30*), can be used as quantum memories (*13*, *31*), and can enable the generation of complex multiphoton entangled states (*32*, *33*). Despite pioneering swapping protocols have been implemented using spin-photon entanglement (*10*) or photon pairs produced by the very same QD (*34*, *35*), to the best of our knowledge, no experiment has demonstrated photonic entanglement swapping with separate quantum emitters. In this work, we implement this pioneering experiment and discuss its prospects for the construction of quantum networks.

[1]Department of Physics, Sapienza University of Rome, Rome 00185, Italy. [2]University of Vienna, Faculty of Physics and Vienna Doctoral School in Physics and Vienna Center for Quantum Science and Technology, Boltzmanngasse 5, A-1090 Vienna, Austria. [3]Austria Christian Doppler Laboratory for Photonic Quantum Computer, University of Vienna, Faculty of Physics, Boltzmanngasse 5, A-1090 Vienna, Austria. [4]Department of Physics, Politecnico di Milano, Milan 20133, Italy. [5]Institute of Semiconductor and Solid-State Physics, Johannes Kepler University Linz, Linz 4040, Austria. [6]Technische Physik, University of Würzburg, Würzburg 97074, Germany. [7]Institute for Photonic Quantum Systems (PhoQS), Center for Optoelectronics and Photonics Paderborn (CeOPP) and Department of Physics, Paderborn University, Paderborn 33098, Germany. [8]Instituto de Fisica Gleb Wataghin, Universidade Estadual de Campinas, Campinas 13083-859, Brazil. [9]Research Centre for Microtechnology FHV, Vorarlberg University of Applied Sciences, Dornbirn 6850, Austria. [10]Institute of Photonics and Quantum Electronics (IPQ) and Center for Integrated Quantum Science and Technology (IQST), Karlsruhe Institute of Technology, Karlsruhe 76131, Germany.
*Corresponding author. Email: giuseppe.ronco@uniroma1.it (G.R.); rinaldo.trotta@uniroma1.it (R.T.)
†These authors contributed equally to this work.

Downloaded from https://www.science.org at KIT Library on November 19, 2026

### A quantum network based on quantum emitters

Figure 1A shows how to implement entanglement swapping with two ideal quantum emitters generating pairs of polarization-entangled photons. The emission process occurs during the radiative cascade from an excited level $|E_2\rangle$ with angular momentum 0 to the ground state $|G\rangle$ through an intermediate, doubly degenerate level $|E_1\rangle$ with angular momentum of ±1. This scheme produces maximally entangled $|\Phi^+\rangle$ Bell states and can describe both real (*23*) and artificial atoms (*24*). It also embraces the general situation where the emitted photons feature different energies. The swapping protocol requires a Bell-state measurement (BSM) on two photons from each source, namely, 2 and 3 in Fig. 1A, which projects the state of the other photons, i.e., 1 and 4 in a maximally entangled state. This can be readily understood by rewriting the joint four-photon state in the Bell state basis

$$|\Psi\rangle_{1234} = |\Phi^+\rangle_{12} \otimes |\Phi^+\rangle_{34}$$
$$= \frac{1}{2}\left(|\Phi^+\rangle_{14}|\Phi^+\rangle_{23} + |\Phi^-\rangle_{14}|\Phi^-\rangle_{23} + |\Psi^+\rangle_{14}|\Psi^+\rangle_{23} + |\Psi^-\rangle_{14}|\Psi^-\rangle_{23}\right) \quad (1)$$

where $|\Psi^\pm\rangle = \frac{1}{\sqrt{2}}(|HV\rangle \pm |VH\rangle)$ and $|\Phi^\pm\rangle = \frac{1}{\sqrt{2}}(|HH\rangle \pm |VV\rangle)$ are the four Bell states in the polarization basis, $H$ and $V$ (see the "Entanglement swapping protocol" section for derivation of Eq. 1). From Eq. 1, it follows that a BSM on photons 2 and 3 projects the state of photons 1 and 4 in one of the Bell states, depending on the outcome of the BSM. The latter can be easily performed via two-photon interference using beam splitters and single-photon detectors, albeit being able to detect only two of the four Bell states ($|\Psi^\pm\rangle$) (*36*). Note that the scheme of Fig. 1A is symmetric and entanglement can be swapped between photons 2 and 3 by performing the BSM on photons 1 and 4.

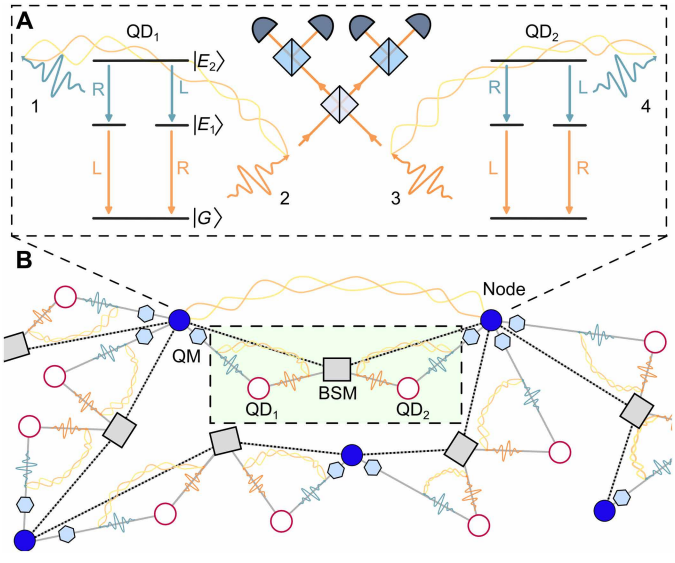



**Fig. 1. Network-ready photonic entanglement swapping.** (**A**) QDs represented as two distinct four-level systems, acting as entangled photon sources. Each system emits two polarization-entangled photons via a radiative cascade initiated by the decay of the excited level $|E_2\rangle$ to the ground state $|G\rangle$, through an intermediate level $|E_1\rangle$. The two QD sources are used to implement entanglement swapping between photons 1 and 4 by performing a Bell-state measurement (BSM) on photons 2 and 3, the latter requiring one beam splitter, two polarizing beam splitters, and single photon detectors. (**B**) Conceptual quantum-network layout in which distinct entangled-photon sources and BSM stations are used to distribute entanglement across distant nodes, depicted as blue circles. Each network node is equipped with quantum memories (QMs). We highlighted quantum (classical) channels with solid (dashed) lines, whereas the dashed light-green rectangle marks the network block pictured in (A).

An entanglement-swapping chain can serve as a building block for quantum repeater networks and, as an example, we envisage here using quantum emitters in protocols that rely on quantum memories (*2*). Figure 1B shows a schematic of such a network, where multiple swapping operations are used to teleport entanglement between different nodes, each of them equipped with quantum memories. It is worth highlighting that the proposed scheme accounts for the different energies of the photons generated during the radiative cascades and, in addition, foresees the same energy for the photons traveling among the different nodes. This is relevant to establish a frequency standard across remote network locations (*37*) and, in principle, allows the same type of quantum memory to be used for all the nodes. The implementation of such a network with quantum emitters presents a series of outstanding challenges, the first being the demonstration of entanglement swapping between remote sources.

Here, we exploit the biexciton (XX)–exciton (X) radiative cascade in QDs. This has been shown to generate quasi-deterministically highly entangled photon pairs (*38*), with high indistinguishability (*39*), record-low multiphoton emission probability (*28*), and, when integrated in photonic cavities (*40*), high efficiency. Moreover, they can be interfaced with quantum memories (*41*), making them particularly suitable for the scheme of Fig. 1A. Despite these advances, there is one main challenge that has so far hampered the demonstration of photonic entanglement swapping: Each QD generates photons with different energy, polarization, and temporal/spectral profile—a direct consequence of the spread in size, shape, and composition of different nanostructures. This feature prevents the use of distinct as-grown QDs to implement BSM based on the interference of indistinguishable photons. Even the most sophisticated growth technique fails to control the QD structural details with atomic precision, given that a single QD is composed of several thousand atoms. Postgrowth tuning techniques must be put in place to precisely reshape the emitted photons, and, in the following, we detail the engineering steps that made the demonstration of photonic entanglement swapping with remote QDs possible.

## RESULTS

### Engineering QDs for entanglement swapping

The device here exploited consists of a GaAs QD (*38*) obtained via droplet-etching epitaxy (*42*) and deterministically positioned at the center of a circular Bragg resonator (CBR) (*40*), in turn, integrated onto a micromachined $[Pb(Mg_{1/3}Nb_{2/3})O_3]_{0.72}$-$[PbTiO_3]_{0.28}$ (PMN-PT) piezoelectric actuator (*27*); see Fig. 2A. The underlying principle of this device is to use the strain fields generated by the PMN-PT to gain control over the energy of the entangled photons, while the CBR cavity reshapes their temporal/spectral profile. The need to control the photon energy can be immediately recognized in Fig. 2 (B and C), which show photoluminescence (PL) spectra of two separate and dissimilar QDs (hereafter referred to as QD1 and QD2) as a function of the electric field $F_p$ applied to the PMN-PT. Without strain ($F_p = 0$ kV / cm), the energies of both X and XX are different.

Downloaded from https://www.science.org at KIT Library on November 19, 2026

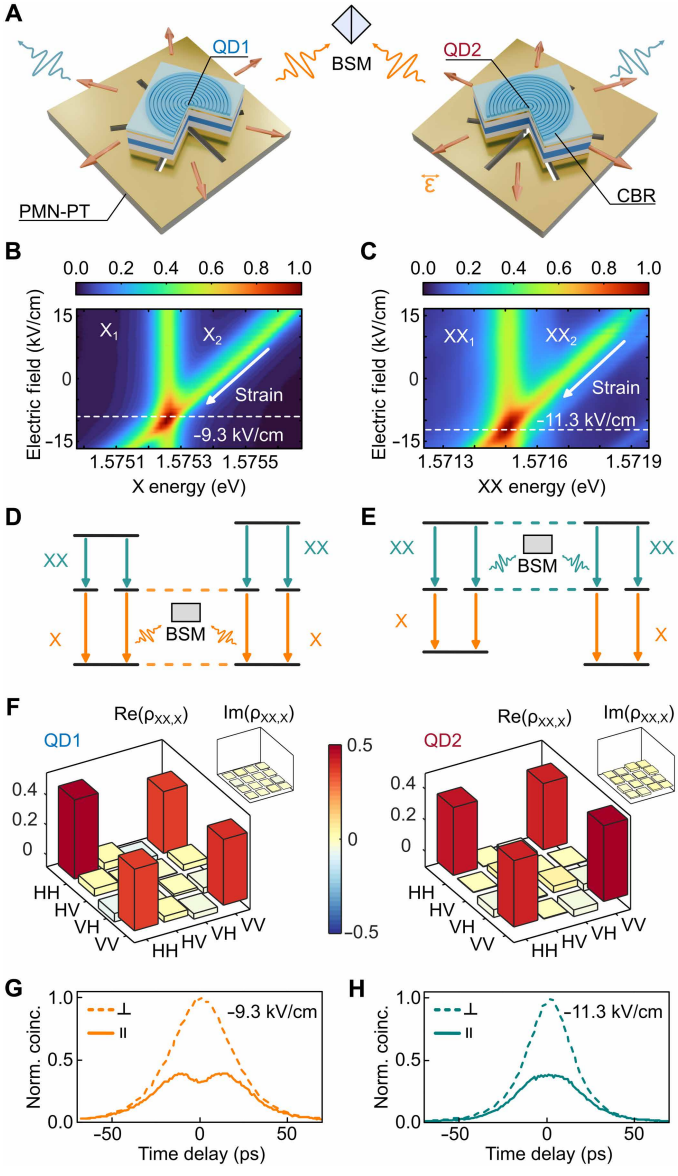



**Fig. 2. Reshaping optical properties of remote QDs for entanglement swapping.** (**A**) Schematics of the interference between photons from two QDs embedded into a circular Bragg resonator (CBR) and integrated onto a piezoelectric actuator (PMN-PT). (**B**) Color-coded μ-PL versus electric field $F_p$ showing energy tuning and crossings for X and (**C**) XX. While QD1 is kept fixed, QD2 is tuned into resonance, achieved at $F_{p,X} = -9.3\ \frac{kV}{cm}$ and $F_{p,XX} = -11.3\ \frac{kV}{cm}$ for the X and XX photons, respectively. (**D**) Remote entanglement swapping schemes for the X and (**E**) the XX. By means of strain tuning, it is possible to bring either the X or the XX of the two QDs in energetic resonance. In (E), for clarity, we have artificially shifted the energy axis in one of the QDs so as to align the XX levels. (**F**) Reconstructed density matrices of the XX-X photon-pairs for QD1 and QD2, respectively, at $F_{p,X}$. (**G**) HOM coincidences histogram at the BS outputs for co- (||) and cross-polarized (⊥) inputs around zero-time delay and for $F_{p,X}$ and (**H**) $F_{p,XX}$.

More specifically, we find that the energy of the X (XX) photons generated by QD1 and QD2 differs by about 120 μeV (160 μeV), corresponding to 2.4 (2.2) times the linewidth extracted from Michelson interferometry (see text S5.4). This substantial detuning would hamper successful BSM and, therefore, entanglement swapping.

To compensate for this detuning, we switch on the electric field $F_p$ across the PMN-PT below QD2 to bring the two X (or XX) transition energies in resonance with sub–micro–electron volt accuracy (*43*). This is shown in Fig. 2 (B and C), which also highlight two additional features. First, we notice that the overall tuning range is as large as 0.5 meV, meaning that it is possible to bring several QDs to emit at the same energy, not only two. Considering that the average spread in energy of the X transitions is about 3 meV, the probability of finding two QDs that can be strain tuned to emit at the same energy is about 7 (see text S5.1, for further details). Second, Fig. 2 (B and C) shows that, when the X of the two QDs are brought into resonance ($F_{p,X} = -9.3\ kV/cm$), the XX transitions still show different energies. The same holds when the XX are tuned in resonance ($F_{p,XX} = -11.3\ kV/cm$), i.e., the two X are found to be at different energies. This evidence is related to the dissimilar XX binding energies (*44*) of the two QDs, a consequence of the different Coulomb interactions among carriers therein confined.

The possibility of using $F_p$ to bring either the X or the XX photons to the same energy turns the swapping scheme of Fig. 1 into the two different configurations shown in Fig. 2 (D and E). More specifically, we can tune $F_p$ to implement entanglement swapping on the XX (X) photons by using the X (XX) photons to perform the BSM, as depicted in Fig. 2D (Fig. 2E). This occurs for $F_{p,X} = -9.3\ kV/cm$ and $F_{p,XX} = -11.3\ kV/cm$, respectively. Once the QD energy levels are strain tuned in one of these configurations, the quality of swapping critically depends on (i) the initial degree of entanglement of the photon pairs and on (ii) the visibility of two-photon interference.

1) We assess the degree of entanglement of the X-XX photons generated by each QD by reconstructing the two-qubit density matrix via quantum-state tomography (*45*). As a quantitative measure of the degree of entanglement, we make use of the fully entangled fraction $f = \max_{\Phi} \langle \Phi | \hat{\rho} | \Phi \rangle$, defined as the largest fidelity to a maximally entangled state (*46*) (for brevity, we refer to it as entanglement fidelity). Figure 2F shows the reconstructed density matrix of the two QDs for $F_{p,X} = -9.3\ kV/cm$, value for which the X energies are matched (see Fig. 2, B and D). They closely resemble two $|\Phi^+\rangle$ states, with an entanglement fidelity of $f_1 = 0.90(2)$ and $f_2 = 0.91(1)$ for QD1 and QD2, respectively. In text S5.3, we also show that the same degree of entanglement is measured when applying $F_{p,XX} = -11.3\ kV/cm$ to bring the XX energy in resonance (see Fig. 2, C and E). For both QDs, we find that the degree of entanglement remains practically constant with $F_p$ (see text S5.3), meaning that our device operates as an energy-tunable source of entangled photons (*47*). This occurs even in the presence of a small residual splitting between the two X states thanks to the acceleration of the transition lifetimes induced by the cavity; see the next point. Across the whole tuning range, the maximum value of the measured fidelity is $f = 0.93(1)$. This points to a small performance gap compared to the state of the art (*38*), likely related to the dynamical optical Stark shift (*48*) and the presence of a nonzero degree of polarization (*49*).

2) Having at hand the possibility to use strain to bring the photons generated by the two QDs in energetic resonance, the visibility of two-photon interference now critically depends on the temporal/spectral overlap of the photon wave-packets (*50*). This, in turn, is connected to the interaction between each QD and the electromagnetic field confined in its own cavity, an effect that can be inferred via the Purcell factor (*40*). It is therefore crucial to ensure that

Downloaded from https://www.science.org at KIT Library on November 19, 2026

similar Purcell factors are obtained for different QDs, a task that requires extremely high accuracy in placing the QD in the center of the CBR cavity, which is also necessary to avoid an undesired degree of polarization (*51*). To tackle this challenge, we use a state-of-the-art imaging technique (*52*) that achieves spatial accuracy of ~15 nm and an overall device yield of ~70%, which is fundamental for the success of this resource-demanding experiment. Here, we highlight that the processing is performed after the transfer of the semiconductor membrane onto the piezoelectric actuator. Despite this additional challenge, we observe an average Purcell factor of $P_X = 7(2)$ [$P_{XX} = 5(1)$] for the X (XX). Considering specifically QD1 and QD2, we estimate similar Purcell factors around 8, with lifetimes of about ~30 ps (~16 ps); see texts S3 and S5.4.

To truly assess the indistinguishability of the photons generated by the two QDs, we exploit Hong-Ou-Mandel interference. We perform experiments when the XX or X energies are tuned by strain to implement the two swapping schemes of Fig. 2 (D and E). In both conditions, we collect coincidences between detectors placed at the output ports of a balanced BS, for co-(||) and cross-polarized (⊥) inputs (see Fig. 2, G and H), prepared using a linear polarizer (*43*). From these measurements, we extract an overall visibility $V$ of two-photon interference of $V_X = 0.43(1)$ and $V_{XX} = 0.46(3)$, which increases to $V_X = 0.48(1)$ and $V_{XX} = 0.51(3)$ if we consider the imperfections of the experimental setup (see text S5.4 for further details). Compared to the previous results obtained for QDs in CBRs (*53*), this represents an improvement by about a factor of 5. The visibilities are instead very similar to those obtained for QDs in bulk (*54*), thus proving that our nanophotonic cavity does not affect the optical quality of the QDs. Our visibilities are now limited by the existence of energy-time entanglement between the photon pairs generated during the cascade (*55*), by the presence of residual charge noise (*24*), persisting differences in photon energy, and nonideal overlap of the photon wave packet; see text S4, for further details. Yet, owing to the sub-20-ps time resolution of our detection apparatus, we can improve the visibilities by temporally postselecting events near zero-time delay (see text S5.4) (*53*). Using a time window of $\Delta t = 10$ ps, the X visibility, for which we can even resolve the dip at zero time delay due to the longer lifetime, increases up to $V_X = 0.66(1)$, whereas, for the XX transition, it reaches $V_{XX} = 0.61(2)$, without taking into account the setup imperfections and multiphoton emission contributions.

### Remote entanglement swapping

Under the conditions described in the previous section, we perform the entanglement swapping protocols of Fig. 2 (D and E). We implement a BSM on the X (XX) photons to swap the entanglement to the XX (X) photons, on which we perform quantum state tomography. Figure 3A shows a schematic of the apparatus in the case of entanglement swapping applied to the XX photons (the protocol works identically for X photons). Considering Eq. 1, the outcome of the BSM on the X photons directly determines the XX Bell state. Specifically, if the BSM returns $|\Psi^-\rangle$ on the X, the XX are found to be in $|\Psi^-\rangle$as well. As we implement the BSM using a BS followed by two polarization-selective BS (PBS; as shown in Fig. 3A), we are able to discriminate only $|\Psi^-\rangle$ (simultaneous detection at AB or CD) and $|\Psi^+\rangle$ (simultaneous detection at AC or BD) states (*56*). This will return $|\Psi^-\rangle$ and $|\Psi^+\rangle$ states for the XX photons, respectively, which can also be evaluated as a function of the temporal window $\Delta t$ we use to postselect the BSM events.

Examples of the recorded density matrices for $\hat{\rho}^{\Psi^\pm}_{XX_1,XX_2}$ are shown in Fig. 3 (B and C) for $\Delta t = 20$ ps. They closely resemble $|\Psi^\pm\rangle$ states, indicating successful entanglement swapping. Figure 3D also confirms that, when the tomography of the XX photons is performed without heralding on the outcome of the BSM, the resulting density matrix resembles a mixture of the four Bell states. We evaluate the entanglement fidelity of the XX photons as a function of $\Delta t$, and we display the obtained results in Fig. 3E. We find that the protocol is successful even without temporal postselection, with a swapping fidelity as large as $f^{\Psi^-}_{swap,XX} = 0.60(1)$ [$f^{\Psi^+}_{swap,XX} = 0.56(1)$]. This value exceeds the classical limit of 0.5 (*57*) by 11 σ (6 σ), unambiguously showing the first successful demonstration of photonic entanglement swapping with remote QD entangled photon-pair sources. Using temporal postselection, the level of entanglement further increases up to $\bar{f}^{\Psi^-}_{swap,XX} = 0.71(2)$ and $\bar{f}^{\Psi^+}_{swap,XX} = 0.65(2)$, always well above the classical limit. As additional confirmation, no entanglement is measured when the QD spectra are detuned from resonance (see text S8.2).

We further demonstrate the protocol by performing the BSM on the XX photons and teleporting entanglement onto the X ones; see Fig. 3F. Without temporal postselection, we record $f^{\Psi^-}_{swap,X} = 0.62(2)$ [$f^{\Psi^+}_{swap,X} = 0.63(2)$], values that are slightly higher than those recorded for the XX photons due to the higher visibility of two photon interference, see text S5.4. Conversely, for $\Delta t = 20$ ps, we obtain similar values within the error bars, i.e., $\bar{f}^{\Psi^-}_{swap,X} = 0.71(3)$ [$\bar{f}^{\Psi^+}_{swap,X} = 0.71(3)$].

To explain the experimental findings, we develop a theoretical model for remote sources that predicts the swapping density matrices with no fitting parameters, but using the measured values of the lifetimes, fine structure splittings (FSSs), and HOM visibilities. The model also takes into account the specific protocol implementation, the use of the polarization-selective BSM as well as the temporal postselection technique, and allows us to derive an analytic form of the swapping matrix (see text S7). From the simulated density matrix, we compute $f_{swap}(\Delta t)$ without free parameters. The predictions, pictured as solid lines in Fig. 3 (E and F), quantitatively reproduce the experimental data and are even able to describe the superior performance for XX-based BSM at large $\Delta t$. The dashed line in Fig. 3 (E and F) is the expected entanglement swapping fidelity taking into account the BS nonideality. After these corrections, we obtain a maximum $f_{swap}$ of 0.73(2) and 0.75(2), respectively, for X and XX BSM.

Owing to the use of CBR cavities, the fourfold coincidence rates that we obtain are more than three orders of magnitude larger than previous attempts focusing on photons from the very same QD (*34*, *35*). For both $|\Psi^\pm\rangle$, we measured swapping rates of a few hertz, see the top axis of Fig. 3 (E and F), which corresponds to a probability of establishing entanglement between uncorrelated photons equal to about $P_{swap} = 2(1) \cdot 10^{-5}$ (see text S6 for further details). Even after temporal postselection, the fourfold coincidence rate remains close to 1 Hz, a direct consequence of the short lifetime of the X and XX transitions.

## DISCUSSION

Our first demonstration of photonic entanglement swapping between two independent and remote quantum emitters marks a major step toward the construction of quantum repeater networks with

Downloaded from https://www.science.org at KIT Library on November 19, 2026

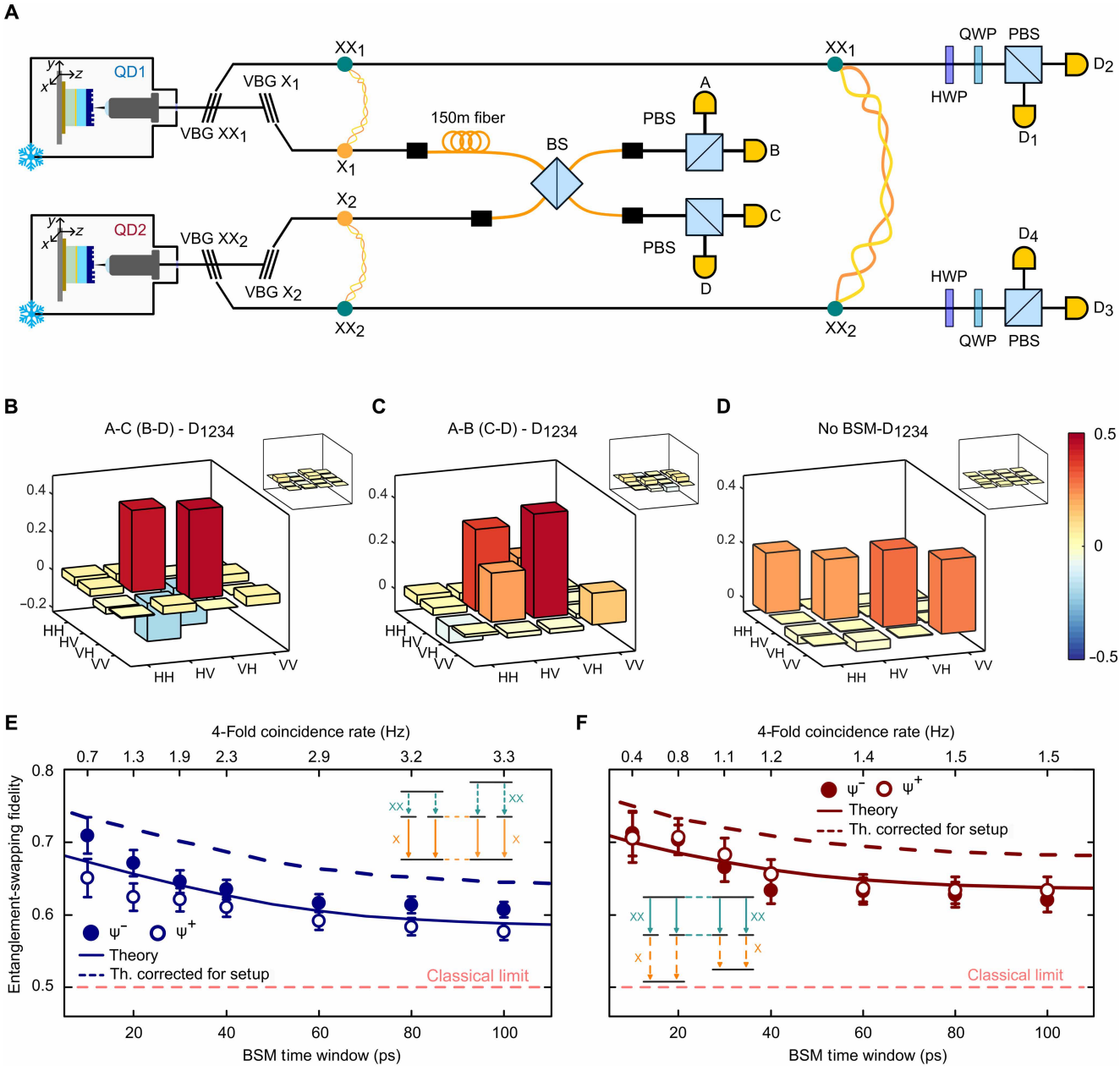



**Fig. 3. Entanglement swapping between remote QDs.** (**A**) Schematic of the swapping setup. The two sources are kept in separate cryostats, and the X and XX emission is collected, redirected, and spectrally filtered through a series of mirrors and volume Bragg gratings (VBGs). Then, the X photons are directed into a BSM setup, and the XX photons are guided to an apparatus for quantum state tomography. We used a 150-m single-mode fiber to demonstrate the feasibility of the protocol in the presence of losses induced by moderate propagation distances in fiber. The same setup can be used to perform the BSM on the XX photons so as to swap entanglement between the X photons. Different combinations of gated coincidences of detectors D1, D2, D3, and D4 with A, B, C, and D provide density matrix for both $|\Psi^+\rangle$ and $|\Psi^+\rangle$ states. (**B**) Real and imaginary part (inset) of the reconstructed density matrices for the swapped XX1-XX2 photons, conditioned on $|\Psi^-\rangle$ and (**C**) $|\Psi^+\rangle$ BSM events, respectively. (**D**) Real and imaginary part (inset) of the same density matrix as obtained without gating on the outcome of the BSM, i.e., on detectors A, B, C, and D. The matrix is diagonal, as expected from an incoherent superposition of Bell states, and shows no degree of entanglement. (**E**) Entanglement swapping fidelity $f_{swap}$ of $|\Psi^{\pm}\rangle$ versus the BSM time window $\Delta t$. The solid line shows the expected values from our theoretical simulations. The dashed line describes the values that could be ideally obtained after correcting for the $g(2)(0)$ and the setup imperfections (see text S7 for further details). The classical limit of 0.5 (red dashed line) is well surpassed even without temporal postselection. The top axis shows the fourfold coincidence rates. The inset shows the energy level scheme used to implement the swapping experiment. (**F**) Same as (E), but for an experiment in which entanglement is swapped between the X photons by performing the BSM on the XX photons.

Downloaded from https://www.science.org at KIT Library on November 19, 2026

nonprobabilistic entangled-photon-pair sources. Within the broader vision of realizing the quantum network displayed in Fig. 1B, future developments should pursue three key objectives: (i) boosting both the entanglement swapping fidelities and rates; (ii) interfacing the swapped photons with suitable quantum memories capable of storing and retrieving polarization qubits; and (iii) deploying the developed technology in urban quantum communication scenarios.

1) Even if the swapping fidelities are unambiguously above the classical limit, advanced quantum communication applications require a higher level of entanglement. As a benchmark, we take a yet-to-be demonstrated quantum key distribution (QKD) protocol with entanglement-swapped photons from remote QDs. To successfully share a secret key between remote network locations, we estimate that it is necessary to have an entanglement fidelity well above 80. This is higher than what we achieved here, but our theoretical and experimental work suggests the path for improvement: Considering the high entanglement of the initial photon pairs, the swapping fidelity is primarily limited by the accuracy of the BSM and, therefore, by the visibility of two-photon interference, as mentioned above. Our visibilities are now limited by the existence of energy-time entanglement (*55*) as well as by the presence of residual charge noise (*24*).

To alleviate this hurdle, one can engineer the ratio between the X and XX lifetimes (*55*) either by designing photonic cavities with differential Purcell enhancement for X and XX (*58*) or by using diode-like structures to control the electric field across the QD (*59*). The first solution has recently been demonstrated on QDs in the same cavity architecture. With this approach, HOM visibility of 90% has been reached. The use of diode structures has demonstrated HOM visibilities as high as 80% without temporal postselection, a value that would allow pushing the swapping fidelity just above the threshold needed to successfully perform QKD. Furthermore, the integration of those diode structures onto CBR has recently been demonstrated, making this approach technologically accessible (*60*, *61*). The electric field can also be used to suppress residual charge noise, with demonstrated HOM visibilities as high as 92 (*62*), albeit in structures with negligible Purcell enhancement and without pumping the XX state for entangled photon generation. The electric field can also be instrumental to increase the overall swapping rates. As discussed in text S6, the presence of blinking in our CBR limits the fourfold coincidence rate by almost a factor of 80. However, recent results (*60*) have demonstrated that blinking can be fully suppressed using electric fields. Therefore, we envisage that the use of diode-like structures in properly designed CBRs will be instrumental to boost the level of entanglement and minimize the number of attempts needed to successfully establish entanglement between remote network nodes. More specifically, in text S6, we estimate that state-of-the-art improvements of the source can push $P_{swap}$ up to 0.17. This value, when using our experimental setup, would result in a coincidence rate close to 3 kHz, already above the value that can be achieved with probabilistic sources of entangled photons (*19*).

2) Interfacing single and entangled photons from QDs with quantum memories is crucial for a functioning quantum network. Several systems can be used for this purpose, such as rare-earth–doped crystals, diamond color centers, and alkali-based quantum memories (*41*). The latter have been used in recent demonstrations of on-demand storage and retrieval of single photons from QDs (*63*), even in combination with CBR cavities (*64*). Despite these advances, additional efforts are needed to improve memory efficiency and storage time and extend its operation to polarization-entangled photons. Modifications of the source are also needed as bandwidth matching is crucial to boost the overall protocol efficiency. The differential Purcell enhancement proposed above is particularly suited for this purpose as the (short) XX photons could be used for the BSM while the (long) X photons could be interfaced with alkali atoms. This type of memory is also interesting for setting a frequency standard across the network (see Fig. 1B). In this case, it would also be necessary to erase the small differences in XX binding energies that we observe in dissimilar QDs (see Fig. 2, B and C, and text S5.3), a task which can be accomplished using the combined effect of strain and electric field (*44*). This would allow turning the swapping schemes of Fig. 2 (D and E) into the universal one shown in Fig. 1A. Last, we want to point out that recent progress on spins confined in GaAs QDs (*31*) shows that quantum memories based on the same hardware shown here could become feasible, with one QD acting as an entangled-photon source and another as a memory.

3) The next step is the exploitation of our entangled photon sources in real-life quantum networks. Given the emission wavelength of our GaAs QDs, free-space quantum links are the ideal choice. Recent demonstrations of entanglement-based QKD (*65*–*67*) as well as quantum teleportation (*53*) suggest that remote entanglement swapping in an urban communication scenario is within reach. Once the source is improved, satellite entanglement-based quantum communication (*68*) is also a path to explore. That said, we point out that our results are also relevant for fiber-based quantum communication. Recent works have shown enormous progress in the performance of single (*69*) and entangled-photon sources (*70*) based on C-band QDs, and our results could be directly transferred to the telecommunication bands. Alternatively, it is also possible to use GaAs QDs in combination with frequency converters, as recently used to implement quantum teleportation (*71*). Therefore, we envisage that our first demonstration of entanglement swapping between remote QDs will now open the path for the construction of large-scale quantum networks that exploit nonprobabilistic entanglement resources to distribute entanglement across distant parties (*68*–*76*).

## MATERIALS AND METHODS

### Optical characterization

The two QDs are hosted at cryogenic temperatures (3.5 and 5 K, respectively) in two independent closed-cycle cryostats. Excitation and collection are performed in back-reflection geometry with a 0.5–numerical aperture aspheric lens, used both to focus the pump and to collect the signal. A Ti:sapphire laser provides 140-fs excitation pulses for both sources at a repetition rate of 80 MHz, doubled using a Mach-Zehnder interferometer. A 4f pulse slicer selects a narrow spectral component, with bandwidth tunable from ~80 μeV to a few hundred micro–electron volts. The bandwidth is chosen to be short enough in the time domain to mitigate the optical Stark shift (*48*), yet spectrally sharp to avoid laser photons overlapping the X and XX energies. Spectral filtering based on the reflection of volume Bragg gratings isolates the X and XX transitions, which are subsequently directed either to the BSM stage or to the quantum-state-tomography setup through optical fibers. For FSS measurements, a half-wave plate and a polarizer are used; the half-wave plate is rotated by π at steps of 2° while synchronizing the acquisition of a charge-coupled device camera placed at the output of a 750-mm spectrometer. In combination with a grating with 1800

Downloaded from https://www.science.org at KIT Library on November 19, 2026

lines per millimeter, the setup achieves a spectral resolution of about 0.02 nm.

### Hong-Ou-Mandel interference

HOM interference between either X or XX photons occurs at the fiber-BS of the BSM setup. The two photons are sent through single-mode fibers to interfere at the BS, and the outputs are directly connected to the superconducting nanowire single-photon detectors (SNSPDs). The excitation pulse from a common laser is divided into two paths using a fiber BS, with one arm including a delay line. By monitoring the coincidence counts between the two photons, we temporally matched the excitation pulses so that the photons arrived simultaneously at the BS. To obtain the histograms shown in Fig. 2 (G and H), we selected a specific component of the FSS and rotated its polarization to align with a common reference axis for both sources. In this configuration, interference occurs only when the photons are indistinguishable. The HOM visibility, defined as the relative depth of the coincidence dip at zero-time delay for parallel-polarized photons with respect to the coincidences for orthogonally polarized photons, was extracted from coincidence histograms acquired under both polarization settings.

Because the visibility is derived from the integrated coincidences around zero delay, we postselected the events within a time window centered at zero-time delay $\tau = 0$ and integrated the coincidence counts over the interval $[-\Delta t, \Delta t]$. The visibility is therefore given by

$$V(\Delta t) = 1 - \frac{C_{\parallel}^{\Delta t}}{C_{\perp}^{\Delta t}}$$

where $C_{\parallel,\perp}^{\Delta t}$ represent the integrated coincidence areas within the selected window. Note that the effective HOM visibility contributing to the BSM operation is lower than the directly measured value, due to chromatic dispersion arising from the finite FSS (see text S5.4).

### Polarization-selective BSM

Thanks to polarization-selective optics, the BSM setup enables discrimination between both $|\Psi^{\pm}\rangle$ Bell states. The apparatus, schematically illustrated in Fig. 3A, consists of a 50:50 fiber BS for HOM interference. The two BS outputs are collimated and directed into free space through two equivalent optical paths, each comprising a PBS followed by a quarter-wave–half-wave–quarter-wave–plate sequence for correcting polarization rotations. The four PBS outputs (labeled as A, B, C, and D) are fiber coupled and sent to SNSPDs featuring an average timing jitter of 15 ps and connected to ultrafast electronics with 2-ps time resolution. The two photons entering the BS are in one of the four Bell states. Consequently, if their joint wave function is in the states $|\Phi^{\pm}\rangle$ or $|\Psi^{+}\rangle$, then they exit through the same output port of the BS, as a result of HOM interference. Conversely, if they are in the state $|\Psi^{-}\rangle$, then they will exit from different ports. At this stage, the two PBSs discriminate co- and cross-polarized photons, leading to distinct coincidence detections. Because the $|\Phi^{\pm}\rangle$ states consist of copolarized photons, they cannot trigger a coincidence event because both photons are routed to the same detector. On the contrary, the $|\Psi^{\pm}\rangle = \frac{1}{\sqrt{2}}(|HV\rangle \pm |VH\rangle)$ states exhibit cross-polarized photons. The state $|\Psi^{+}\rangle$ will thus yield coincidences between pairs of detectors at the outputs of the same PBS (i.e., A-B or C-D). Conversely, the $|\Psi^{-}\rangle$ state will generate coincidences between orthogonally polarized photons at the outputs of different PBSs (i.e., A-C or B-D) (*56*). These coincidences serve as gate counts for gating the quantum state tomography on the remaining photons.

### Entanglement swapping protocol

Consider two entangled photon pairs in the Bell state $|\Phi^{+}\rangle = \frac{1}{\sqrt{2}}(|HH\rangle \pm |VV\rangle)$. If we label the four photonic modes as 1, 2, 3, and 4, the four-photon state can be written as

$$\begin{aligned}|\Psi\rangle_{1,2,3,4} &= |\Phi^{+}\rangle_{1,2} \cdot |\Phi^{+}\rangle_{3,4} \\ &= \frac{1}{\sqrt{2}}\left(|HH\rangle_{1,2} \pm |VV\rangle_{1,2}\right) \cdot \frac{1}{\sqrt{2}}\left(|HH\rangle_{3,4} \pm |VV\rangle_{3,4}\right) \\ &= \frac{1}{2}\left(|HHHH\rangle_{1,2,3,4} + |VVVV\rangle_{1,2,3,4} + |HHVV\rangle_{1,2,3,4} + |VVHH\rangle_{1,2,3,4}\right)\end{aligned}$$

This four-photon state can be expressed as a linear combination of products of Bell states. In particular, $\frac{1}{2}(|HHHH\rangle_{1,2,3,4} + |VVVV\rangle_{1,2,3,4}) = |\Phi+\rangle_{1,4} \cdot |\Phi^{+}\rangle_{2,3} + |\Phi^{-}\rangle_{1,4} \cdot |\Phi^{-}\rangle_{2,3}$ and $\frac{1}{2}(|HHVV\rangle_{1,2,3,4} + |VVHH\rangle_{1,2,3,4}) = \frac{1}{2}(|HV\rangle_{1,4}|HV\rangle_{2,3} + |VH\rangle_{1,4}|VH\rangle_{2,3}) = |\Psi^{+}\rangle_{1,4} \cdot |\Psi^{+}\rangle_{2,3} + |\Psi^{-}\rangle_{1,4} \cdot |\Psi^{-}\rangle_{2,3}$. Substituting these relations in the expression for $|\Psi\rangle_{1,2,3,4}$, one obtains the four-photon state in Eq. 1.

## Supplementary Materials

**This PDF file includes:**

Supplementary Text
Figs. S1 to S11
References

## REFERENCES


1. H. J. Kimble, The quantum internet. *Nature* **453**, 1023–1030 (2008).
2. H. J. Briegel, W. Dür, J. I. Cirac, P. Zoller, Quantum repeaters: The role of imperfect local operations in quantum communication. *Phys. Rev. Lett.* **81**, 5932–5935 (1998).
3. K. Azuma, S. E. Economou, D. Elkouss, P. Hilaire, L. Jiang, H.-K. Lo, I. Tzitrin, Quantum repeaters: From quantum networks to the quantum internet. *Rev. Mod. Phys.* **95**, 045006 (2023).
4. K. S. Choi, H. Deng, J. Laurat, H. J. Kimble, Mapping photonic entanglement into and out of a quantum memory. *Nature* **452**, 67–71 (2008).
5. K. Azuma, K. Tamaki, H.-K. Lo, All-photonic quantum repeaters. *Nat. Commun.* **6**, 6787 (2015).
6. M. Żukowski, A. Zeilinger, M. A. Horne, A. K. Ekert, "Event-ready-detectors" Bell experiment via entanglement swapping. *Phys. Rev. Lett.* **71**, 4287–4290 (1993).
7. N. Sangouard, C. Simon, H. de Riedmatten, N. Gisin, Quantum repeaters based on atomic ensembles and linear optics. *Rev. Mod. Phys.* **83**, 33–80 (2011).
8. C. H. Bennett, G. Brassard, C. Crépeau, R. Jozsa, A. Peres, W. K. Wootters, Teleporting an unknown quantum state via dual classical and Einstein-Podolsky-Rosen channels. *Phys. Rev. Lett.* **70**, 1895–1899 (1993).
9. J.-W. Pan, D. Bouwmeester, H. Weinfurter, A. Zeilinger, Experimental entanglement swapping: Entangling photons that never interacted. *Phys. Rev. Lett.* **80**, 3891–3894 (1998).
10. A. Delteil, Z. Sun, W. Gao, E. Togan, S. Faelt, A. Imamoğlu, Generation of heralded entanglement between distant hole spins. *Nat. Phys.* **12**, 218–223 (2016).
11. R. Stockill, M. J. Stanley, L. Huthmacher, E. Clarke, M. Hugues, A. J. Miller, C. Matthiesen, C. Le Gall, M. Atatüre, Phase-tuned entangled state generation between distant spin qubits. *Phys. Rev. Lett.* **119**, 010503 (2017).
12. G. Guccione, T. Darras, H. Le Jeannic, V. B. Verma, S. W. Nam, A. Cavaillès, J. Laurat, Connecting heterogeneous quantum networks by hybrid entanglement swapping. *Sci. Adv.* **6**, eaba4508 (2020).
13. M. Pompili, S. L. N. Hermans, S. Baier, H. K. C. Beukers, P. C. Humphreys, R. N. Schouten, R. F. L. Vermeulen, M. J. Tiggelman, L. dos Santos Martins, B. Dirkse, S. Wehner, R. Hanson, Realization of a multinode quantum network of remote solid-state qubits. *Science* **372**, 259–264 (2021).
14. T. van Leent, M. Bock, F. Fertig, R. Garthoff, S. Eppelt, Y. Zhou, P. Malik, M. Seubert, T. Bauer, W. Rosenfeld, W. Zhang, C. Becher, H. Weinfurter, Entangling single atoms over 33 km telecom fibre. *Nature* **607**, 69–73 (2022).


Downloaded from https://www.science.org at KIT Library on November 19, 2026

15. J.-L. Liu, X.-Y. Luo, Y. Yu, C.-Y. Wang, B. Wang, Y. Hu, J. Li, M.-Y. Zheng, B. Yao, Z. Yan, D. Teng, J.-W. Jiang, X.-B. Liu, X.-P. Xie, J. Zhang, Q.-H. Mao, X. Jiang, Q. Zhang, X.-H. Bao, J.-W. Pan, Creation of memory–memory entanglement in a metropolitan quantum network. *Nature* **629**, 579–585 (2024).
16. S. Bartolucci, P. Birchall, H. Bombín, H. Cable, C. Dawson, M. Gimeno-Segovia, E. Johnston, K. Kieling, N. Nickerson, M. Pant, F. Pastawski, T. Rudolph, C. Sparrow, Fusion-based quantum computation. *Nat. Commun.* **14**, 912 (2023).
17. R. Kaltenbaek, R. Prevedel, M. Aspelmeyer, A. Zeilinger, High-fidelity entanglement swapping with fully independent sources. *Phys. Rev. A* **79**, 040302 (2009).
18. Y. Tsujimoto, K. Wakui, T. Kishimoto, S. Miki, M. Yabuno, H. Terai, M. Fujiwara, G. Kato, Experimental entanglement swapping through single-photon $\chi(2)$ nonlinearity. *Nat. Commun.* **16**, 8720 (2025).
19. R. B. Jin, M. Takeoka, U. Takagi, R. Shimizu, M. Sasaki, Highly efficient entanglement swapping and teleportation at telecom wavelength. *Sci. Rep.* **5**, 9333 (2015).
20. H. de Riedmatten, I. Marcikic, J. A. W. van Houwelingen, W. Tittel, H. Zbinden, N. Gisin, Long-distance entanglement swapping with photons from separated sources. *Phys. Rev. A* **71**, 050302 (2005).
21. H. Takesue, B. Miquel, Entanglement swapping using telecom-band photons generated in fibers. *Opt. Express* **17**, 10748–10756 (2009).
22. Q.-C. Sun, Y.-L. Mao, Y.-F. Jiang, Q. Zhao, S.-J. Chen, W. Zhang, W.-J. Zhang, X. Jiang, T.-Y. Chen, L.-X. You, L. Li, Y.-D. Huang, X.-F. Chen, Z. Wang, X. Ma, Q. Zhang, J.-W. Pan, Entanglement swapping with independent sources over an optical-fiber network. *Phys. Rev. A* **95**, 032306 (2017).
23. A. Aspect, J. Dalibard, G. Roger, Experimental test of Bell's inequalities using time-varying analyzers. *Phys. Rev. Lett.* **49**, 1804–1807 (1982).
24. N. Tomm, A. Javadi, N. O. Antoniadis, D. Najer, M. C. Löbl, A. R. Korsch, R. Schott, S. R. Valentin, A. D. Wieck, A. Ludwig, R. J. Warburton, A bright and fast source of coherent single photons. *Nat. Nanotechnol.* **16**, 399–403 (2021).
25. D. D. Awschalom, R. Hanson, J. Wrachtrup, B. B. Zhou, Quantum technologies with optically interfaced solid-state spins. *Nat. Photonics* **12**, 516–527 (2018).
26. M. Kianinia, Z.-Q. Xu, M. Toth, I. Aharonovich, Quantum emitters in 2D materials: Emitter engineering, photophysics, and integration in photonic nanostructures. *Appl. Phys. Rev.* **9**, 011306 (2022).
27. M. B. Rota, T. M. Krieger, Q. Buchinger, M. Beccaceci, J. Neuwirth, H. Huet, N. Horová, G. Lovicu, G. Ronco, S. F. Covre da Silva, G. Pettinari, M. Moczała-Dusanowska, C. Kohlberger, S. Manna, S. Stroj, J. Freund, X. Yuan, C. Schneider, M. Ježek, S. Höfling, F. Basso Basset, T. Huber-Loyola, A. Rastelli, R. Trotta, A source of entangled photons based on a cavity-enhanced and strain-tuned GaAs quantum dot. *eLight* **4**, 13 (2024).
28. L. Schweickert, K. D. Jöns, K. D. Zeuner, S. F. Covre da Silva, H. Huang, T. Lettner, M. Reindl, J. Zichi, R. Trotta, A. Rastelli, V. Zwiller, On-demand generation of background-free single photons from a solid-state source. *Appl. Phys. Lett.* **112**, 093106 (2018).
29. W. B. Gao, P. Fallahi, E. Togan, J. Miguel-Sanchez, A. Imamoğlu, Observation of entanglement between a quantum dot spin and a single photon. *Nature* **491**, 426–430 (2012).
30. K. De Greve, L. Yu, P. L. McMahon, J. S. Pelc, C. M. Natarajan, N. Y. Kim, E. Abe, S. Maier, C. Schneider, M. Kamp, S. Höfling, R. H. Hadfield, A. Forchel, M. M. Fejer, Y. Yamamoto, Quantum-dot spin–photon entanglement via frequency downconversion to telecom wavelength. *Nature* **491**, 421–425 (2012).
31. M. H. Appel, A. Ghorbal, N. Shofer, L. Zaporski, S. Manna, S. F. C. da Silva, U. Haeusler, C. Le Gall, A. Rastelli, D. A. Gangloff, M. Atatüre, A many-body quantum register for a spin qubit. *Nat. Phys.* **21**, 368–373 (2025).
32. D. Cogan, Z.-E. Su, O. Kenneth, D. Gershoni, Deterministic generation of indistinguishable photons in a cluster state. *Nat. Photonics* **17**, 324–329 (2023).
33. H. Huet, P. R. Ramesh, S. C. Wein, N. Coste, P. Hilaire, N. Somaschi, M. Morassi, A. Lemaître, I. Sagnes, M. F. Doty, O. Krebs, L. Lanco, D. A. Fioretto, P. Senellart, Deterministic and reconfigurable graph state generation with a single solid-state quantum emitter. *Nat. Commun.* **16**, 4337 (2025).
34. M. Zopf, R. Keil, Y. Chen, J. Yang, D. Chen, F. Ding, O. G. Schmidt, Entanglement swapping with semiconductor-generated photons violates Bell's inequality. *Phys. Rev. Lett.* **123**, 160502 (2019).
35. F. Basso Basset, M. B. Rota, C. Schimpf, D. Tedeschi, K. D. Zeuner, S. F. Covre da Silva, M. Reindl, V. Zwiller, K. D. Jöns, A. Rastelli, R. Trotta, Entanglement swapping with photons generated on demand by a quantum dot. *Phys. Rev. Lett.* **123**, 160501 (2019).
36. N. Lütkenhaus, J. Calsamiglia, K.-A. Suominen, Bell measurements for teleportation. *Phys. Rev. A* **59**, 3295–3300 (1999).
37. N. Akopian, R. Trotta, E. Zallo, S. Kumar, P. Atkinson, A. Rastelli, O. G. Schmidt, V. Zwiller, An artificial atom locked to natural atoms. arXiv:1302.2005 (2013).
38. D. Huber, M. Reindl, S. F. Covre da Silva, C. Schimpf, J. Martín-Sánchez, H. Huang, G. Piredda, J. Edlinger, A. Rastelli, R. Trotta, Strain-tunable GaAs quantum dot: A nearly dephasing-free source of entangled photon pairs on demand. *Phys. Rev. Lett.* **121**, 033902 (2018).
39. D. Huber, M. Reindl, Y. Huo, H. Huang, J. S. Wildmann, O. G. Schmidt, A. Rastelli, R. Trotta, Highly indistinguishable and strongly entangled photons from symmetric GaAs quantum dots. *Nat. Commun.* **8**, 15506 (2017).
40. J. Liu, R. Su, Y. Wei, B. Yao, S. F. C. da Silva, Y. Yu, J. Iles-Smith, K. Srinivasan, A. Rastelli, J. Li, X. Wang, A solid-state source of strongly entangled photon pairs with high brightness and indistinguishability. *Nat. Nanotechnol.* **14**, 586–593 (2019).
41. J. Neuwirth, F. Basso Basset, M. B. Rota, E. Roccia, C. Schimpf, K. D. Jöns, A. Rastelli, R. Trotta, Quantum dot technology for quantum repeaters: From entangled photon generation toward the integration with quantum memories. *Mater. Quantum Technol.* **1**, 043001 (2021).
42. M. Gurioli, Z. Wang, A. Rastelli, T. Kuroda, S. Sanguinetti, Droplet epitaxy of semiconductor nanostructures for quantum photonic devices. *Nat. Mater.* **18**, 799–810 (2019).
43. R. Trotta, E. Zallo, C. Ortix, P. Atkinson, J. D. Plumhof, J. Van Den Brink, A. Rastelli, O. G. Schmidt, Universal recovery of the energy-level degeneracy of bright excitons in InGaAs quantum dots without a structure symmetry. *Phys. Rev. Lett.* **109**, 147401 (2012).
44. R. Trotta, E. Zallo, E. Magerl, O. G. Schmidt, A. Rastelli, Independent control of exciton and biexciton energies in single quantum dots via electroelastic fields. *Phys. Rev. B* **88**, 155312 (2013).
45. D. F. V. James, P. G. Kwiat, W. J. Munro, A. G. White, Measurement of qubits. *Phys. Rev. A* **64**, 052312 (2001).
46. J. Grondalski, D. M. Etlinger, D. F. V. James, The fully entangled fraction as an inclusive measure of entanglement applications. *Phys. Lett. A* **300**, 573–580 (2002).
47. R. Trotta, J. Martín-Sánchez, J. S. Wildmann, G. Piredda, M. Reindl, C. Schimpf, E. Zallo, S. Stroj, J. Edlinger, A. Rastelli, Wavelength-tunable sources of entangled photons interfaced with atomic vapours. *Nat. Commun.* **7**, 10375 (2016).
48. F. Basso Basset, M. B. Rota, M. Beccaceci, T. M. Krieger, Q. Buchinger, J. Neuwirth, H. Huet, S. Stroj, S. F. Covre da Silva, G. Ronco, C. Schimpf, S. Höfling, T. Huber-Loyola, A. Rastelli, R. Trotta, Signatures of the optical Stark effect on entangled photon pairs from resonantly pumped quantum dots. *Phys. Rev. Lett.* **131**, 166901 (2023).
49. A. Laneve, M. B. Rota, F. Basso Basset, M. Beccaceci, V. Villari, T. Oberleitner, Y. Reum, T. M. Krieger, Q. Buchinger, R. Prasad, S. F. C. da Silva, A. Pfenning, S. Stroj, S. Höfling, A. Rastelli, T. Huber-Loyola, R. Trotta, Wavevector-resolved polarization entanglement from radiative cascades. *Nat. Commun.* **16**, 6209 (2025).
50. T. Legero, T. Wilk, A. Kuhn, G. Rempe, Time-resolved two-photon quantum interference. *Appl. Phys. B* **77**, 797–802 (2003).
51. G. Peniakov, Q. Buchinger, M. Helal, S. Betzold, Y. Reum, M. B. Rota, G. Ronco, M. Beccaceci, T. M. Krieger, S. F. C. da Silva, A. Rastelli, R. Trotta, A. Pfenning, S. Höfling, T. Huber-Loyola, Polarized and unpolarized emission from a single emitter in a bullseye resonator. *Laser Photonics Rev.* **18**, 2300835 (2024).
52. Q. Buchinger, C. Krause, A. Zhang, G. Peniakov, M. Helal, Y. Reum, A. T. Pfenning, S. Höfling, T. Huber-Loyola, Deterministic quantum dot cavity placement using hyperspectral imaging with high spatial accuracy and precision. *Nano Converg.* **12**, 36 (2025).
53. A. Laneve, G. Ronco, M. Beccaceci, P. Barigelli, F. Salusti, N. Claro-Rodriguez, G. De Pascalis, A. Suprano, L. Chiaudano, E. Schöll, L. Hanschke, T. M. Krieger, Q. Buchinger, S. F. Covre da Silva, J. Neuwirth, S. Stroj, S. Höfling, T. Huber-Loyola, M. A. Usuga Castaneda, G. Carvacho, N. Spagnolo, M. B. Rota, F. Basso Basset, A. Rastelli, F. Sciarrino, K. D. Jöns, R. Trotta, Quantum teleportation with dissimilar quantum dots over a hybrid quantum network. *Nat. Commun.* **16**, 10028 (2025).
54. M. Reindl, K. D. Jöns, D. Huber, C. Schimpf, Y. Huo, V. Zwiller, A. Rastelli, R. Trotta, Phonon-assisted two-photon interference from remote quantum emitters. *Nano Lett.* **17**, 4090–4095 (2017).
55. E. Schöll, L. Schweickert, L. Hanschke, K. D. Zeuner, F. Sbresny, T. Lettner, R. Trivedi, M. Reindl, S. F. Covre da Silva, R. Trotta, J. J. Finley, J. Vučković, K. Müller, A. Rastelli, V. Zwiller, K. D. Jöns, Crux of using the cascaded emission of a three-level quantum ladder system to generate indistinguishable photons. *Phys. Rev. Lett.* **125**, 233605 (2020).
56. F. Basso Basset, F. Salusti, L. Schweickert, M. B. Rota, D. Tedeschi, S. F. Covre da Silva, E. Roccia, V. Zwiller, K. D. Jöns, A. Rastelli, R. Trotta, Quantum teleportation with imperfect quantum dots. *npj Quantum Inf.* **7**, 7 (2021).
57. A. G. White, A. Gilchrist, G. J. Pryde, J. L. O'Brien, M. J. Bremner, N. K. Langford, Measuring two-qubit gates. *J. Opt. Soc. Am. B.* **24**, 172–183 (2007).
58. R. Behrends, M. v. Helversen, P. K. Saha, L. Rickert, K. Kaymazlar, M. Lach, N. D. Kewitz, J. Kaupp, Y. Reum, T. Huber-Loyola, S. Höfling, A. Pfenning, T. Heindel, Highly-indistinguishable single-photons at 1550 nm from a two-photon resonantly excited Purcell-enhanced quantum dot. arXiv:2602.06140 (2026).
59. G. Undeutsch, M. Aigner, A. J. Jr, J. Garcia, M. Reindl, S. Peter, C. Mader, S. F. Weidinger, S. Covre da Silva, S. Manna, E. Schöll, and A. Rastelli. Electric-field control of photon indistinguishability in cascaded decays in quantum dots. *Nano Lett.* **25**, 7121–7127 (2025).
60. I. Brytavskyi, T. Oberleitner, C. Weidinger, M. Aigner, G. Undeutsch, T. Steindl, J. Reindl, A. Garcia Jr., M. Peter, C. Schimpf, S. Manna, M. B. Rota, Q. Buchinger, S. Höfling, T. Huber-Loyola, R. Trotta, T. M. Krieger, E. Schöll, A. Rastelli, A diode nanocavity for fast,


Downloaded from https://www.science.org at KIT Library on November 19, 2026

efficient and tunable emission of highly entangled photon pairs and Fourier-transform-limited single photons. arXiv:2607.11494 [quant-ph] (2026).
61. P. Gschwandtner, Q. Buchinger, K. Chand Maurya, M. Helal, B. Souza Damasceno, R. Kumar, H. Kim, I. Brytavskyi, S. Kuhn, A. Ludwig, D. Reuter, Y.-H. Cho, T. Huber-Loyola, S. Höfling, Purcell enhanced and blinking free single photons from InAs/GaAs quantum dots in deterministically placed circular Bragg gratings. arXiv:2607.11495v2 [cond-mat.mes-hall] (2026).
62. L. Zhai, G. N. Nguyen, C. Spinnler, J. Ritzmann, M. C. Löbl, A. D. Wieck, A. Ludwig, A. Javadi, R. J. Warburton, Quantum interference of identical photons from remote GaAs quantum dots. *Nat. Nanotechnol.* **17**, 829–833 (2022).
63. S. E. Thomas, L. Wagner, R. Joos, R. Sittig, C. Nawrath, P. Burdekin, I. M. de Buy Wenniger, M. J. Rasiah, T. Huber-Loyola, S. Sagona-Stophel, S. Höfling, M. Jetter, P. Michler, I. A. Walmsley, S. L. Portalupi, P. M. Ledingham, Deterministic storage and retrieval of telecom light from a quantum dot single-photon source interfaced with an atomic quantum memory. *Sci. Adv.* **10**, eadi7346 (2024).
64. B. Maaß, A. Barua, N. V. Ewald, E. Robertson, K. Gaur, S. I. Park, S. Rodt, J.-D. Song, S. Reitzenstein, J. Wolters, Storage of single photons from a semiconductor quantum dot in a room-temperature atomic vapor memory with on-demand retrieval. *Quantum Sci. Technol.* **10**, 035058 (2025).
65. F. Basso Basset, M. Valeri, J. Neuwirth, E. Polino, M. B. Rota, D. Poderini, C. Pardo, G. Rodari, E. Roccia, S. F. Covre da Silva, G. Ronco, N. Spagnolo, A. Rastelli, G. Carvacho, F. Sciarrino, R. Trotta, Daylight entanglement-based quantum key distribution with a quantum dot source. *Quantum Sci. Technol.* **8**, 025002 (2023).
66. F. Basso Basset, M. Valeri, E. Roccia, V. Muredda, D. Poderini, J. Neuwirth, N. Spagnolo, M. B. Rota, G. Carvacho, F. Sciarrino, R. Trotta, Quantum key distribution with entangled photons generated on demand by a quantum dot. *Sci. Adv.* **7**, eabe6379 (2021).
67. F. Basso Basset, R. Trotta, Quantum dots for entanglement-based quantum key distribution. *Appl. Phys. Rev.* **13**, 021339 (2026).
68. Y.-A. Chen, Q. Zhang, T.-Y. Chen, W.-Q. Cai, S.-K. Liao, J. Zhang, K. Chen, J. Yin, J.-G. Ren, Z. Chen, S.-L. Han, Q. Yu, K. Liang, F. Zhou, X. Yuan, M.-S. Zhao, T.-Y. Wang, X. Jiang, L. Zhang, W.-Y. Liu, Y. Li, Q. Shen, Y. Cao, C.-Y. Lu, R. Shu, J.-Y. Wang, L. Li, N.-L. Liu, F. Xu, X.-B. Wang, C.-Z. Peng, J.-W. Pan, An integrated space-to-ground quantum communication network over 4,600 kilometres. *Nature* **589**, 214–219 (2021).
69. N. Hauser, M. Bayerbach, J. Kaupp, Y. Reum, G. Peniakov, J. Michl, M. Kamp, T. Huber-Loyola, A. T. Pfenning, S. Höfling, S. Barz, Deterministic and highly indistinguishable single photons in the telecom C-band. *Nat. Commun.* **17**, 537 (2026).
70. T. Lettner, S. Gyger, K. D. Zeuner, L. Schweickert, S. Steinhauer, C. Reuterskiöld Hedlund, S. Stroj, A. Rastelli, M. Hammar, R. Trotta, K. D. Jöns, V. Zwiller, Strain-controlled quantum dot fine structure for entangled photon generation at 1550 nm. *Nano Lett.* **21**, 10501–10506 (2021).
71. T. Strobel, M. Vyvlecka, I. Neureuther, T. Bauer, M. Schäfer, S. Kazmaier, N. L. Sharma, R. Joos, J. H. Weber, C. Nawrath, W. Nie, G. Bhayani, C. Hopfmann, C. Becher, P. Michler, S. L. Portalupi, Telecom-wavelength quantum teleportation using frequency-converted photons from remote quantum dots. *Nat. Commun.* **16**, 10027 (2025).
72. B. Kambs, C. Becher, Limitations on the indistinguishability of photons from remote solid state sources. *New J. Phys.* **20**, 115003 (2018).
73. V. Giesz, S. L. Portalupi, T. Grange, C. Antón, L. De Santis, J. Demory, N. Somaschi, I. Sagnes, A. Lemaître, L. Lanco, A. Auffèves, P. Senellart, Cavity-enhanced two-photon interference using remote quantum dot sources. *Phys. Rev. B* **92**, 161302 (2015).
74. J.-P. Jahn, M. Munsch, L. Béguin, A. V. Kuhlmann, M. Renggli, Y. Huo, F. Ding, R. Trotta, M. Reindl, O. G. Schmidt, A. Rastelli, P. Treutlein, R. J. Warburton, An artificial Rb atom in a semiconductor with lifetime-limited linewidth. *Phys. Rev. B* **92**, 245439 (2015).
75. C. Schimpf, S. Manna, S. F. Covre da Silva, M. Aigner, A. Rastelli, Entanglement-based quantum key distribution with a blinking-free quantum dot operated at a temperature up to 20 K. *Adv. Photonics* **3**, 065001 (2021).
76. H. Wang, H. Hu, T.-H. Chung, J. Qin, X. Yang, J.-P. Li, R.-Z. Liu, H.-S. Zhong, Y.-M. He, X. Ding, Y.-H. Deng, Q. Dai, Y.-H. Huo, S. Höfling, C.-Y. Lu, J.-W. Pan, On-demand semiconductor source of entangled photons which simultaneously has high fidelity, efficiency, and indistinguishability. *Phys. Rev. Lett.* **122**, 113602 (2019).
77. C. Schimpf, M. Reindl, D. Huber, B. Lehner, S. F. Covre da Silva, S. Manna, M. Vyvlecka, P. Walther, A. Rastelli, Quantum cryptography with highly entangled photons from semiconductor quantum dots. *Sci. Adv.* **7**, eabe8905 (2021).
78. B. T. Kirby, S. Santra, V. S. Malinovsky, M. Brodsky, Entanglement swapping of two arbitrarily degraded entangled states. *Phys. Rev. A* **94**, 012336 (2016).
79. C. Schimpf, F. Basso Basset, M. Aigner, W. Attenender, L. Ginés, G. Undeutsch, M. Reindl, D. Huber, D. Gangloff, E. A. Chekhovich, C. Schneider, S. Höfling, A. Predojević, R. Trotta, A. Rastelli, Hyperfine interaction limits polarization entanglement of photons from semiconductor quantum dots. *Phys. Rev. B* **108**, L081405 (2023).
80. A. J. Hudson, R. M. Stevenson, A. J. Bennett, R. J. Young, C. A. Nicoll, P. Atkinson, K. Cooper, D. A. Ritchie, A. J. Shields, Coherence of an entangled exciton-photon state. *Phys. Rev. Lett.* **99**, 266802 (2007).
81. J. Řeháček, Z. Hradil, E. Knill, A. I. Lvovsky, Diluted maximum-likelihood algorithm for quantum tomography. *Phys. Rev. A* **75**, 042108 (2007).

**Acknowledgments:** We thank P. Mataloni for the fruitful discussions, A. Miriametro for the technical contribution, and K. Broccoletti for administrative support. **Funding:** This project has received funding from the European Union's Horizon 2020 research and innovation program under grant agreement no. 899814, Qurope project (R.T., F.B.B., K.D.J., A.R., and M.B.R.), and no. 871130, Ascent+ project (A.R.); from the QuantERA II program that has received funding from the European Union's Horizon 2020 research and innovation program under grant agreement no. 101017733 via the project QDE-QKD (R.T., A.L., F.B.B., S.H., T.H.-L., and A.R.); and from the European Union's Horizon Europe research and innovation program under EPIQUE Project GA no. 101135288 (R.T., M.B., F.C., A.L., and M.B.R.). We also acknowledge support from MUR (Ministero dell'Università e della Ricerca) through the PNRR MUR project PE0000023-NQSTI (R.T., F.B.B., and M.B.R.) and the European Commission by project QUID (Quantum Italy Deployment) funded in the Digital Europe Programme under the grant agreement no. 101091408 (R.T., G.R., P.B., and F.B.B.). A.R. acknowledges support of the EU HE EIC Pathfinder challenges action under grant agreement no. 101115575 (Q-ONE), from the QuantERA program via the project MEEDGARD (FFG grant no. 906046), the Austrian Science Fund (FWF) (10.55776/COE1, FG5, PIN4389523) via the Research Group FG5 (10.55776/FG5), and the cluster of excellence Quantum Science Austria (quantA) (10.55776/COE1), as well as the Linz Institute of Technology (LIT), and the LIT Secure and Correct Systems Lab, supported by the State of Upper Austria. T.H.-L. acknowledges funding from the German Federal Ministry of Research, Technology and Space (BMFTR), through the project Qecs (FKZ: 13 N16272). This work is supported by the Deutsche Forschungsgemeinschaft (German Research Foundation) through the transregional collaborative research center TRR142/3-2022 (231447078) (F.S. and K.D.J.) and the European Research Council starting grant (LiNQs, 101042672) (F.S. and K.D.J.). S.F.C.d.S. acknowledges São Paulo Research Foundation (FAPESP), Brazil, process no. 2024/08527-2 and 2024/21615-8 for financial support. **Author contributions:** M.B. and G.R. performed the experiment with the contribution of F.C., P.B., and A.L. under the supervision of M.B.R. and R.T. M.B.R. developed the data acquisition code with the help of F.S. and K.D.J. M.B., G.R., F.C., P.B., and M.B.R. analyzed the data. M.B. performed the theoretical analysis with the help of F.B.B. S.F.C.d.S. and A.R. designed and grew the QD sample. M.B.R., T.M.K., T.O., Q.B., B.S.D., and S.K. designed and processed the circular Bragg-Resonator under the supervision of R.T., A.R., T.H.-L., and S.H. S.S. processed the micromachined piezoelectric actuator. G.R. and R.T. wrote the paper with contributions from all the authors. R.T. conceived the experiment and coordinated the project. **Competing interests:** The authors declare that they have no competing interests. **Data, code, and materials availability:** All data and code needed to evaluate and reproduce the results in the paper are present in the paper and/or the Supplementary Materials. This study did not generate new materials.

Submitted 3 April 2026
Accepted 5 October 2026
Published 6 November 2026
10.1126/sciadv.aeh7797

Downloaded from https://www.science.org at KIT Library on November 19, 2026

ScienceAdvances

# Photonic entanglement swapping with remote quantum dots

Mattia Beccaceci, Giuseppe Ronco, Fabrizio Cienzo, Pierpaolo Bassetti, Alessandro Laneve, Francesco Basso Basset, Tobias M. Krieger, Thomas Oberleitner, Quirin Buchinger, Francesco Salusti, Barbara Souza Damasceno, Silke Kuhn, Saimon F. Covre da Silva, Sandra Stroj, Klaus D. Jöns, Sven Höfling, Tobias Huber-Loyola, Armando Rastelli, Michele B. Rota, and Rinaldo Trotta

*Sci. Adv.* **12** (45), eaeh7797. DOI: 10.1126/sciadv.aeh7797

**View the article online**
https://www.science.org/doi/10.1126/sciadv.aeh7797
**Permissions**
https://www.science.org/help/reprints-and-permissions

Downloaded from https://www.science.org at KIT Library on November 19, 2026

Use of this article is subject to the Terms of service

*Science Advances* (ISSN 2375-2548) is published by the American Association for the Advancement of Science. 1200 New York Avenue NW, Washington, DC 20005. The title *Science Advances* is a registered trademark of AAAS.

Copyright © 2026 The Authors, some rights reserved; exclusive licensee American Association for the Advancement of Science. No claim to original U.S. Government Works. Distributed under a Creative Commons Attribution NonCommercial License 4.0 (CC BY-NC).